Chimica Techno Acta
published by Ural Federal University
eISSN 2411-1414
chimicatechnoacta.ru

ARTICLE
2023, vol. 10(1), No. 202310108
DOI: 10.15826/chimtech.2023.10.1.08

Optical response of $SrTiO_3$ thin films grown via a sol-gel-hydrothermal method

Yulia Eka Putri [a]*, Tio Putra Wendari [a], Restu Aulia Arham [a], Melvi Muharmi [a], Dedi Satria [b], Rahmayeni Rahmayeni [a], Diana Vanda Wellia [a]

a: Department of Chemistry, Faculty of Mathematics and Natural Sciences, Andalas University, Padang 25163, Indonesia
b: Department of Pharmacy, Muhammadiyah University of Sumatera Barat, Padang 25172, Indonesia
* Corresponding author: yuliaekaputri@sci.unand.ac.id

This paper belongs to a Regular Issue.

Abstract

The polycrystalline $SrTiO_3$ thin films were prepared by the sol-gel-hydrothermal method on glass substrates. The synthesis pathway was initiated by preparing a clear TiO_2 solution using the sol-gel method. This clear solution was then deposited on a glass substrate using the dip coating technique, followed by the transformation of a thin layer of TiO_2 into $SrTiO_3$ by the hydrothermal method. The crystal structure, bond interactions, and band gap energy of $SrTiO_3$ thin layers were characterized using X-ray Diffraction (XRD), Fourier Transform Infra-Red spectroscopy (FTIR), and UV–Vis Diffuse Reflectance Spectroscopy (UV-DRS). The XRD patterns of all $SrTiO_3$ thin layers indicated the perovskite structure of the samples. The FTIR spectrum showed an interaction of the silanol groups on the surface of the glass substrate with Ti–O–Ti of $SrTiO_3$ layers. The characteristics of the UV-DRS spectrum were influenced by the thickness of the $SrTiO_3$ layer formed on the glass substrate. The findings of this work provide insights for producing $SrTiO_3$ layers with specified thickness and morphology.

Keywords

$SrTiO_3$
thin film
perovskite
hydrothermal
optical properties

Received: 18.12.22
Revised: 12.01.23
Accepted: 16.01.23
Available online: 23.01.23

Key findings

- $SrTiO_3$ thin films were synthesized using the sol-gel-hydrothermal method.
- The hydrothermal synthesis time affected the purity of the $SrTiO_3$ thin film.
- The optical bandgap of $SrTiO_3$ was influenced by the specified thickness of the samples.

1. Introduction

Two-dimensional (2-dimensional/2D) nanomaterials in the form of thin layers have attracted significant attention because of the successful isolation of graphene into sheet forms. Thin films are currently employed in various fields to develop their capabilities [1]. 2D materials have several advantages, such as having layers with a thin atomic-scale arrangement, large surface area, strong mechanical properties, and good electrical and thermal conductivities [2]. This is the main attraction for preparing 2D nanomaterials with good physical and chemical properties and using them in various applications [3].

Metal oxide-based perovskite structures are an important and attractive class because of their wide application range. The strontium titanate ($SrTiO_3$) semiconductor compound has a typical metal oxide perovskite structure with the Pm3m space group of at room temperature. Inside the perovskite structure, Sr^{2+} ions are in the corners and Ti^{4+} ions in the centers of the cube, while O^{2-} anions surround Ti^{4+} ions to form a regular octahedron in the cubic symmetry. Each Sr^{2+} ion is surrounded by four TiO_6 octahedra and coordinated by twelve O^{2-} ions, whereas the Ti^{4+} ion is sixfold coordinated by the O^{2-} ion [4]. In the TiO_6 octahedra, the hybridization of the O-2p state with the Ti-3d state results in a pronounced covalent bonding, whereas the Sr^{2+} and O^{2-} ions exhibit ionic bonding characteristics. Therefore, $SrTiO_3$ has mixed ionic-covalent bonding properties [5]. This type of chemical bonding leads to a unique structure, which can be a

model for electronic materials. In an ideal $SrTiO_3$ perovskite structure, there is a flexible ionic arrangement making it easy to modify. So, the structural instability creates new properties and improves the optical and electrical properties [6].

$SrTiO_3$ thin films are amongthe perovskite oxides with various advantages, including catalytic activities [7], electrical and dielectric properties [8], ferroelectric properties [9], and a possibility of using them as lattice-matched substrates for high-T_c oxide superconductors [10]. One of the strategies to improve its promising properties is the thin film fabrication techniques. Several thin film growth technique have been reported, such as sputtering [11], sol-gel [12], pulsed laser ablation [13], and chemical vapor deposition [14]. On the other hand, substrate selection is crucial because the substrate greatly affects the quality of the film. Glass, fluorine-doped tin oxide (FTO), indium-doped tin oxide (ITO), silicon, and metal substrates have been used to fabricate $SrTiO_3$ thin films [15].

This work adopted a two-stage sol-gel-hydrothermal technique to deposit $SrTiO_3$ thin films on the glass substrate. The first stage was depositing a TiO_2 layer on a glass substrate. Then the second stage was the conversion of the TiO_2 thin film into $SrTiO_3$ on the same substrate. Synthesis of TiO_2 was performed by the sol-gel method. TiO_2 was deposited on the glass substrate by the dip coating method. Afterward, the $SrTiO_3$ layer was formed by the hydrothermal method. In forming $SrTiO_3$ thin films using the hydrothermal method, the effect of $Sr(OH)_2{\cdot}8H_2O$ concentration on the structure and the optical response was identified by varying the concentration of $Sr(OH)_2{\cdot}8H_2O$ precursor solution. Then, X-Ray Diffraction (XRD) was utilized to analyze the structure and crystallinity of the synthesized sample. Difuse-Reflectance Ultra Violet Visible (DRS UV-Vis) and Fourier Transform Infra-Red (FTIR) spectroscopy methods were also employed to determine optical properties by calculating band gap values and the interaction between the synthesized compound and the glass substrate, respectively.

2. Materials and method

2.1. Chemicals

The materials used in this study were titanium tetrachloride ($TiCl_4$) (Sigma-Aldrich 0.09 M in 20% HCl), ammonium hydroxide (NH_4OH) (Pudac Scientific 25%), hydrogen peroxide (H_2O_2) (Merck 30%), distilled water, ethanol (C_2H_5OH) (Merck ≥ 97.5%), silver nitrate ($AgNO_3$) (Sigma-Aldrich), strontium hydroxide octahydrate ($Sr(OH)_2{\cdot}8H_2O$) (Sigma-Aldrich), ice cube, and commercially available glass substrates (76.2 mm × 25.4 mm × 1 mm).

2.2. Instrumentation

The tools used in this study were glassware, analytical scales, pipettes, stirring rods, spatulas, pH paper, ice baths, magnetic stirrer (IKA C-MAG HS 7), oven, autoclaves, Teflon vessel, XRD diffractometer PANalytical X'pert PRO, DRS UV-Vis spectrometer Specord 210 Plus Analytic Jena, and FTIR (Fourier Transform Infra-Red spectrometer) Shimadzu-IR Prestige 21.

2.3. Synthesis of TiO_2 gel precursor

The TiO_2 gel precursor solution was synthesized by dropwise addition of 36 mL $TiCl_4$ into 300 mL of distilled water in an ice water bath while stirring using a magnetic stirrer for 30 min. Then, the 25% NH_4OH solution was added dropwise to adjust the pH of the solution to 7 under stirring for 24 h. The solution was then centrifuged to separate the precipitate and filtrate. The resulting precipitate was washed using distilled water until no Cl^- ions remained. The presence of Cl^- ions remaining in the solution was detected by adding $AgNO_3$ solution to the remaining washing water until no white precipitate of AgCl was formed. 80 mL of distilled water and 28 mL of H_2O_2 were added to the white free of Cl^- precipitate dropwise while stirring using a magnetic stirrer. The mixed solution was then stirred for 4 h until a transparent yellow solution was formed. The color was because of the TiO_2 gel precursor [16].

2.4. Deposition of TiO_2 thin films on glass substrate

The used glass substrate was commercial glass with the size of 76.2 mm × 25.4 mm × 1 mm. 4 preparatory glass sheets were cleaned using the ultrasonication method in distilled water, acetone, isopropanol, and ethanol, for 15 min in each. The clean glass was dried at room temperature. Then, the TiO_2 layer was deposited on the glass substrate using the dip coating method. The glass substrate was dipped for 30 s into the TiO_2 gel precursor and then withdrawn with a withdrawal speed of 0.1 cm/s. Afterward, it was dried for 5 min at 100 °C. This procedure was repeated 5 times to achieve several nanolayers of TiO_2. After that, the TiO_2-coated glass substrate was further dried for 1 h at 120 °C and labeled TOFT. Next, a sheet of TOFT sample was calcined at 500 °C and cooled by normal cooling for 1 h to ensure the formation of TiO_2 on the glass substrate. This calcined TOFT sample was labeled TOFK.

2.5. Transformation of TiO2 thin films into $SrTiO_3$ thin films

The transformation of the TiO_2 thin layer sample into $SrTiO_3$ was conducted by preparing a strontium solution, $Sr(OH)_2{\cdot}8H_2O$, with varying concentrations of 25 mM, 50 mM, and 75 mM. Then, the solution was placed into the autoclave Teflon vessel; the glass substrate coated with TiO_2 thin films was placed in a vertical position. The hydrothermal process was conducted at 150 °C for 3 h. After the hydrothermal process was completed, the thin film on the glass substrate was removed from the autoclave and calcined at 600 °C for 30 min. The synthesized $SrTiO_3$ thin films were labeled STOF-25, STOF-50, and STOF-75.

 DOI: 10.15826/chimtech.2023.10.1.08

3. Results and Discussion

The $SrTiO_3$ thin films were synthesized in-situ using two methods. Firstly, the TiO_2 precursors were synthesized using the sol-gel method and then deposited on a glass substrate using the dip-coating method. Secondly, the $SrTiO_3$ thin films were synthesized using the hydrothermal method through the diffusion of Sr^{2+} on the TiO_2 layer. The resulting $SrTiO_3$ thin film product is a layer that grows evenly on the substrate with good transparency because the color of the glass substrate coated with $SrTiO_3$ is not much different from that of the glass substrate. The differences in the physical shapes of the glass substrate, the TiO_2 thin layer, and the $SrTiO_3$ thin layer are shown in Figure 1. This image shows the changes that occurred in the coating process. It can be seen that the glass substrate coated with the TiO_2 thin layer still looks transparent (Figure 1b). However, after being coated with $SrTiO_3$, all samples of the $SrTiO_3$ film appear slightly opaque (translucent) (Figure 1d, e, f).

The TiO_2 layer synthesized by the sol-gel method was in an amorphous form. Therefore, a sintering process was conducted to ensure the formation of crystalline TiO_2. TiO_2 in the amorphous phase can be altered into a crystalline phase by the sintering process. So, the crystalline TiO_2 was characterized by XRD to determine its crystal structure, as shown in Figure 2. The TOFT XRD pattern shows that this thin layer is amorphous because no specific peaks appear. However, the TOFK sample showed diffraction peaks at the 2θ values of 25.2°, 47.8°, and 54.9° indexed as (101), (200), and (105). These diffraction peaks correspond to the anatase TiO_2 phase based on the ICSD standard No. 9855 [17]. This proves that the thin film TiO_2 synthesized by the sol-gel method was successfully formed as a TiO_2 gel. Therefore, it can be used as a precursor for synthesizing $SrTiO_3$.

Furthermore, the $SrTiO_3$ thin layer samples synthesized by the hydrothermal method were characterized by XRD. The diffraction patterns are shown in Figure 3. The XRD patterns show that the STOF-50 and STOF-75 samples exhibited $SrTiO_3$ diffraction peaks. Meanwhile, STOF-25 samples did not show any $SrTiO_3$ diffraction peaks with only $SrCO_3$ diffraction peaks as impurities.

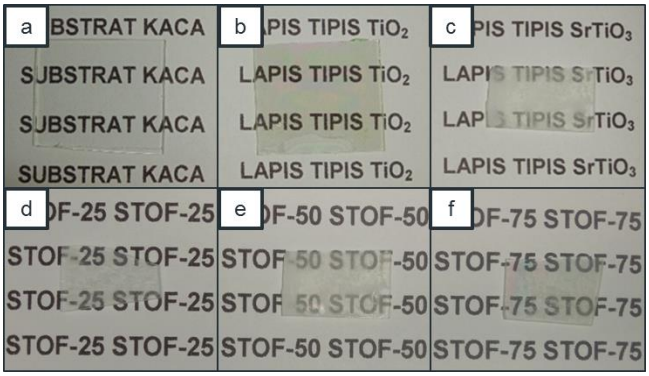

Figure 1 Physical appearance of glass substrate (a), TiO_2 thin film (b), $SrTiO_3$ thin film (c), STOF-25 (d), STOF-50 (e), STOF-75 (f).

The absence of $SrTiO_3$ in the STOF-25 is due to the lower concentration of Sr^{2+} than the amount sufficient for the stoichiometric formation of $SrTiO_3$. Meanwhile, the presence of diffraction peaks in the plane (110) for the STOF-50 and STOF-75 samples indicates that $SrTiO_3$ formed on the surface of the glass substrate. The shift of plane (110) towards smaller 2θ can be caused by several factors, such as (1) lattice strain, (2) sintering process at high temperature, and (3) mismatch of thermal expansion between the $SrTiO_3$ compound and the used glass substrate [18].

Also, the emergence of $SrCO_3$ diffraction peaks is due to the possible reaction of the dissolved CO_2 in the autoclave with the Sr^{2+} ions during the synthesis. This is due to the interaction between Sr^{2+} and the dissolved CO_2 in the aqueous solution. Theoretically, hydrated alkaline earth solutions ($(SrOH)_2{\cdot}8H_2O$) have a high solubility in the presence of carbonate ions (CO_3^{2-}) because the solution is alkaline.

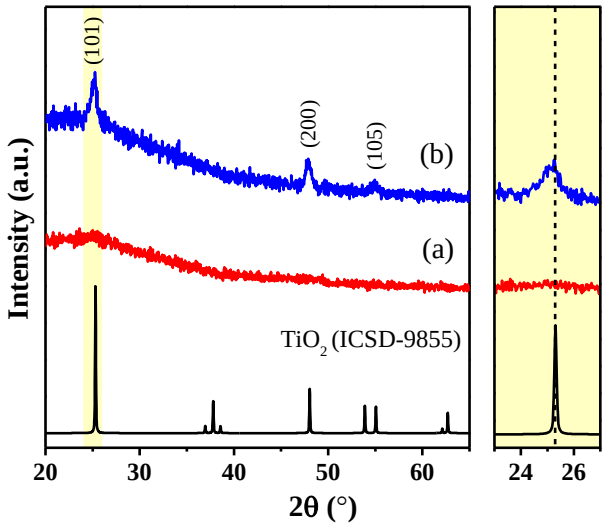

Figure 2 XRD patterns of TiO_2 thin films before sintering (TOFT) (a) and TiO_2 thin films after sintering (TOFK) (b).

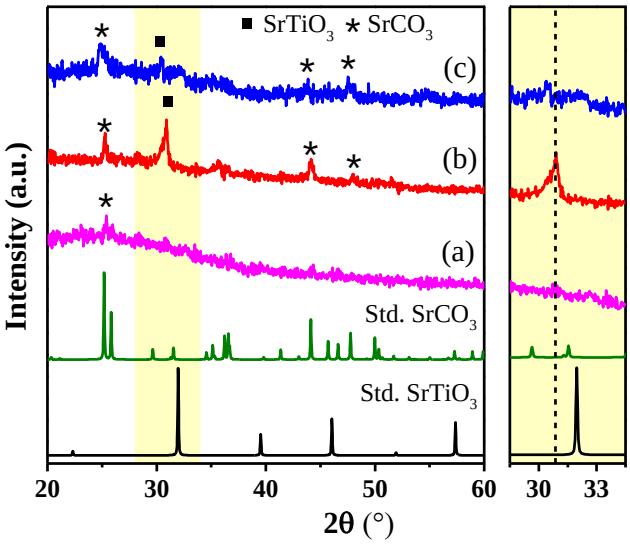

Figure 3 XRD pattern of $SrTiO_3$ thin films: STOF-25 (a), STOF-50 (b) and STOF-75 (c).

 DOI: 10.15826/chimtech.2023.10.1.08

Then, water absorption also causes the strontium to become more alkaline. So, the Sr^{2+} ions are likely to combine with OH^- ions to form $SrOH^+$ and absorb CO_2 in the autoclave during the hydrothermal process. The absorbed CO_2 is then converted to CO_3^{2-} and reacts with hydrated strontium to form $SrCO_3$ impurities [19].

Functional group analysis using FTIR aims to determine the presence of interactions in the successfully synthesized STOF-50 and STOF-75 samples. Figure 4 shows the FTIR spectrum of the glass substrate and the synthesized samples in the wave number range of 400–1600 cm^{-1}. The obtained spectra for the glass substrate and the STOF-50 and STOF-75 samples show specific peaks of their functional groups. The FTIR spectrum of the glass substrate showed the presence of the Si–O stretching vibration of the silanol (Si–OH) group at the wave number of 917 cm^{-1} [20], and the stretching vibration of Si–O in the siloxane (Si–O–Si) group at the wave number of 766 cm^{-1} [21]. The silanol stretching vibrations were also observed in the spectrum of STOF-50 and STOF-75 samples; however, these peaks shifted to the wavenumber of 903 cm^{-1} (STOF-50) and 892 cm^{-1} (STOF-75). The shift in the wave number of silanol functional groups is due to the strong interaction between the surface of the glass substrate through the silanol present in the surface glass with Ti–O–Ti present in the $SrTiO_3$ compound. The intense interaction results in the formation of new chemical bonds through the terminal groups Si–O–H with Ti–O–Ti to produce Si–O–Ti along the surface of the glass substrate and $SrTiO_3$ film. The formation of Si–O–Ti is further strengthened by changes in the intensity of the FTIR spectrum by weakening the silanol peaks in STOF-50 samples and STOF-75, indicating a stronger Si–O–Ti bond. Furthermore, the appearance of a new peak at a wavenumber of 478 cm^{-1} in the STOF-50 and STOF-75 spectrum refers to the Ti–O stretching vibration of the Ti–O–Ti of TiO_6 octahedral in the $SrTiO_3$ compound [22].

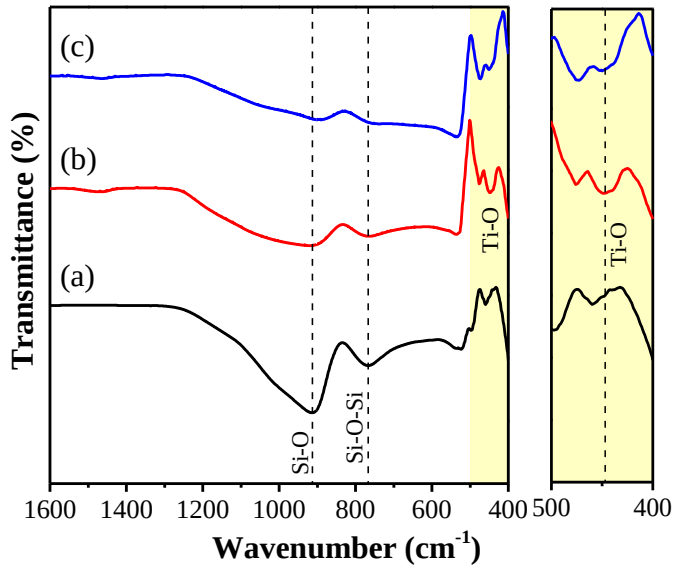

Figure 4 FTIR spectrum of glass substrate (a), STOF-50 (b) and STOF-75 (c).

DRS UV-Vis analysis was performed to analyze the optical properties of the STOF-50 and STOF-75 samples based on the band gap energy values, as shown in Figure 5a. Both samples demonstrate a good absorbance in UV light at around 325 nm and a weak absorbance in visible light. The STOF-75 sample shows a higher peak intensity than the STOF-50 sample. These results show that the absorbance value is directly proportional to the $SrTiO_3$ concentration on the glass substrate, as the absorbance of the STOF-75 is greater than that of STOF-50 [23]. The obtained band gap for each sample was calculated using the Tauc-Mott (MT) method from the UV-DRS absorption spectrum, according to the following equation:

$$(\alpha h\nu)^2 = A(h\nu - E_g), \quad (1)$$

where A is the side width parameter, α is the absorption coefficient, h is Plank's constant (J·s), and E_g is the bandgap energy (eV).

Figure 5b shows the optical band gap energy of the samples using Tauc plots of the STOF-50 and STOF-75 thin film samples at 2.50 eV and 3.58 eV, respectively. The difference in these values is due to the presence of impurities in the sample, as confirmed by the XRD pattern, and the thickness of the thin layer, known from the absorption of the UV-DRS spectrum.

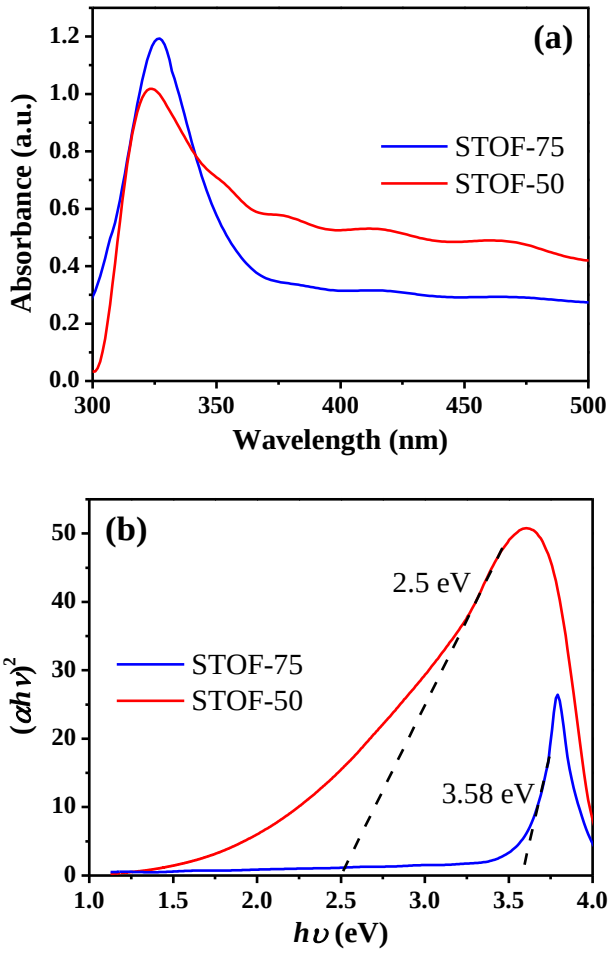

Figure 5 UV-Vis spectrum of $SrTiO_3$ thin films (a) and optical band gap energy (b).

 DOI: 10.15826/chimtech.2023.10.1.08

According to the XRD pattern and UV-DRS spectrum, it is known that the STOF-75 sample contains $SrCO_3$ impurities, and its absorption is greater than that of the STOF-50 sample. Therefore, the band gap energy value of the STOF-75 sample is greater than that of the STOF-50 [15].

4. Limitations

In this study, $SrTiO_3$ thin films were not single-phase because $SrCO_3$ was found as an impurity. So, the crystallinity of the samples remained low. Therefore, future research will focus on forming single-phase $SrTiO_3$ thin films by adjusting several hydrothermal synthesis parameters, such as variations in temperature, time, and the concentration of the starting material.

5. Conclusions

$SrTiO_3$ thin films were synthesized using the sol-gel-hydrothermal method. The concentration of Sr^{2+} in the solution affected the growth of $SrTiO_3$ on a glass substrate, where the STOF-50 and STOF-75 formed a thin layer of $SrTiO_3$. However, the presence of $SrTiO_3$ was not found in the STOF-25 because the strontium solution concentration was insufficient. The FTIR spectrum showed an interaction between the glass substrate and $SrTiO_3$ with the appearance of silanol groups. The STOF-50 and STOF-75 samples had a good absorbance in UV light and a very weak absorbance in visible light with band gap values of 2.50 eV and 3.58 eV, respectively.

• Supplementary materials

No supplementary materials are available.

• Funding

The author would like to thank the Faculty of Mathematics and Natural Sciences, Universitas Andalas, through the PNBP Fund Research Grant No.16/UN.16.03.D/PP/FMIPA/2021.

• Acknowledgments

None.

• Author contributions

Conceptualization: Y.E.P.
Visualization: T.P.W.
Investigation: R.A.A., M.M.
Methodology: Y.E.P., D.V.W.
Supervision: R.R., D.V.W.
Writing – original draft: Y.E.P.
Writing – review & editing: D.S.

• Conflict of interest

The authors declare no conflict of interest.

• Additional information

Author IDs:
Yulia Eka Putri, Scopus ID 55261197300;
Tio Putra Wendari, Scopus ID 57208920083;
Dedi Satria, Scopus ID 57200695552;
Rahmayeni Rahmayeni, Scopus ID 55544632300;
Diana Vanda Wellia, Scopus ID 35363286300.

Websites:
Andalas University, https://www.unand.ac.id;
Muhammadiyah University of Sumatera Barat, https://www.umsb.ac.id.

References

1. Britnell L, Ribeiro RM, Eckmann A, Jalil R, Belle BD, Mishchenko A, et al. Strong light-matter interactions in heterostructures of atomically thin films. Sci. 2013;340(6138):1311–1314. doi:10.1126/science.1235547
2. Das S, Kim M, Lee JW, Choi W. Synthesis, properties, and applications of 2-D materials: a comprehensive review. Crit Rev Solid State Mater Sci. 2014;39(4):231–252. doi:10.1080/10408436.2013.836075
3. Fiori G, Bonaccorso F, Iannaccone G, Palacios T, Neumaier D, Seabaugh A, et al. Electronics based on two-dimensional materials. Nat Nanotechnol. 2014;9(10):768–779. doi:10.1016/j.ceramint.2021.11.075
4. Putri YE, Wendari TP, Rahmah AA, Refinel R, Said SM, Sofyan N, et al. Tuning the morphology of $SrTiO_3$ nanocubes and their enhanced electrical conductivity. Ceram Int. 2022 Feb 15;48(4):5321–6. doi:10.1016/j.ceramint.2021.11.075
5. Trejgis K, Dramićanin MD, Marciniak L. Highly sensitive multiparametric luminescent thermometer for biologically-relevant temperatures based on Mn^{4+}, Ln^{3+} Co-doped $SrTiO_3$ nanocrystals. J Alloys Compd. 2021;875. doi:10.1016/j.jallcom.2021.159973
6. Gastiasoro MN, Ruhman J, Fernandes RM. Superconductivity in dilute $SrTiO_3$: a review. Ann Phys. 2020;417:168107. doi:10.1016/j.aop.2020.168107
7. Riemke FC, Ücker CL, Carreño NLV, da Silva Cava S, Teixeira MP, Fajardo HV, et al. Influence of Nb_2O_5 grown on $SrTiO_3$ nanoseeds in the catalytic oxidation of thioanisole. Mater Chem Phys. 2022;278:125591. doi:10.1016/j.matchemphys.2021.125591
8. Bhogra A, Masarrat A, Meena R, Hasina D, Bala M, Dong CL, et al. Tuning the electrical and thermoelectric properties of N ion implanted $SrTiO_3$ Thin films and their conduction mechanisms. Sci Rep. 2019;9(1):1–11. doi:10.1038/s41598-019-51079-y
9. Song H, Son JY. Examining imprinted ferroelectric hysteresis loops and improved energy storage properties of Mn-doped epitaxial $SrTiO_3$ thin films using heat treatment. Mater Sci Eng B Solid-State Mater Adv Technol. 2022;285:115925. doi:10.1016/j.mseb.2022.115925
10. Ahadi K, Galletti L, Li Y, Salmani-Rezaie S, Wu W, Stemmer S. enhancing superconductivity in $SrTiO_3$ films with strain. Sci Adv. 2019:1–6. doi:10.1126/sciadv.aaw0120
11. Hadj Youssef A, Ambriz Vargas F, Amaechi I, Sarkissian A, Merlen A, Thomas R, et al. Impact of negative oxygen ions on the deposition processes of RF-magnetron sputtered $SrTiO_3$ thin films. Thin Solid Films. 2018;661:23–31. doi:10.1016/j.tsf.2018.05.054
12. Diao C, Li H, Yang Y, Hao H, Yao Z, Liu H. Significantly improved energy storage properties of sol-gel derived mn-modified $SrTiO_3$ thin films. Ceram Int. 2019;45(9):11784–11791. doi:10.1016/j.ceramint.2019.03.056

 DOI: 10.15826/chimtech.2023.10.1.08

13. Jung F, Delmdahl R, Heymann A, Fischer M, Karl H. Surface evolution of crystalline $SrTiO_3$, $LaAlO_3$ and $Y_3Al_5O_{12}$ targets during pulsed laser ablation. Appl Phys A Mater Sci Process. 2022;128(9):750. doi:10.1007/s00339-022-05805-5
14. He C, Bu X, Yang S, He P, Ding G, Xie X. Core-shell $SrTiO_3$ /graphene structure by chemical vapor deposition for enhanced photocatalytic performance. Appl Surf Sci. 2018;436:373–381. doi:10.1016/j.apsusc.2017.12.063
15. Łęcki T, Zarębska K, Sobczak K, Skompska M. Photocatalytic degradation of 4-chlorophenol with the use of $FTO/TiO_2/SrTiO_3$ composite prepared by microwave-assisted hydrothermal method. Appl Surf Sci. 2019;470:991–1002. doi:10.1016/j.apsusc.2018.11.200
16. Pratiwi N, Zulhadjri, Arief S, Wellia DV. A facile preparation of transparent ultrahydrophobic glass via TiO_2/Octadecyltrichlorosilane (ODTS) coatings for self-cleaning material. Chem Sel. 2020;5(4):1450–1454. doi:10.1002/slct.201904153
17. Taherniya A, Raoufi D. Thickness dependence of structural, optical and morphological properties of sol-gel derived TiO_2 thin film. Nanotechnol. 2018;29(27):1–19. doi:10.1088/2053-1591/aae4d0
18. Zhao J, Deng Y, Wei H, Zheng X, Yu Z, Shao Y, et al. Strained hybrid perovskite thin films and their impact on the intrinsic stability of perovskite solar cells. Sci Adv. 2017;3(11). doi:10.1126/sciadv.aao5616
19. Hong J, Heo SJ, Singh P. Water mediated growth of oriented single crystalline $SrCO_3$ nanorod arrays on strontium compounds. Sci Rep. 2021;11(1):1–11. doi:10.1038/s41598-021-82651-0
20. Dimitriadi M, Zafiropoulou M, Zinelis S, Silikas N, Eliades G. Silane reactivity and resin bond strength to lithium disilicate ceramic surfaces. Dent Mater. 2019;35(8):1082–1094. doi:10.1016/j.dental.2019.05.002
21. Aguiar H, Serra J, González P, León B. Structural study of sol-gel silicate glasses by IR and Raman spectroscopies. J Non Cryst Solids. 2009;355(8):475–480. doi:10.1016/j.jnoncrysol.2009.01.010
22. Yao M, Li F, Peng Y, Chen J, Su Z, Yao X. Enhanced electrical characteristics of sol–gel-derived amorphous $SrTiO_3$ films. J Mater Sci Mater Electron. 2017;28(5):4044–4050. doi:10.1007/s10854-016-6018-8
23. Dulian P, Nachit W, Jaglarz J, Zięba P, Kanak J, Żukowski W. Photocatalytic methylene blue degradation on multilayer transparent TiO_2 coatings. Opt Mater (Amst). 2019;90:264–272. doi:10.1016/j.optmat.2019.02.041

 DOI: 10.15826/chimtech.2023.10.1.08